



Experimentally simulated sea level rise destabilizes carbon-mineral associations in temperate tidal marsh soil

Sean Fettrow^{ID} · Rodrigo Vargas^{ID} ·
Angelia L. Seyfferth^{ID}

Received: 13 July 2022 / Accepted: 23 January 2023 / Published online: 7 February 2023
© The Author(s), under exclusive licence to Springer Nature Switzerland AG 2023

Abstract How sea level rise (SLR) alters carbon (C) dynamics in tidal salt marsh soils is unresolved. Changes in hydrodynamics could influence organo-mineral associations, influencing dissolved organic carbon (DOC) fluxes. As SLR increases the duration of inundation, we hypothesize that lateral DOC export will increase due to reductive dissolution of C-bearing iron (Fe) oxides, destabilizing soil C stocks and influencing greenhouse gas emissions. To test this, soil cores (0–8 cm depth) were collected from the high marsh of a temperate salt marsh that currently experiences changes in water level and soil redox oscillation due to spring-neap tides. Mesocosms experimentally simulated SLR by continuously inundating high marsh soils and were compared to mesocosms with Control conditions, where the water level oscillated on a spring-neap cycle. Porewater DOC, lateral DOC, and porewater reduced Fe (Fe^{2+}) concentrations were significantly higher in SLR treatments (1.7 ± 0.5 mM, 0.63 ± 0.14 mM, and 0.15 ± 0.11 mM, respectively) than Control

treatments (1.2 ± 0.35 mM, 0.56 ± 0.15 mM, and 0.08 ± 0.01 mM, respectively). Solid phase analysis with Fe extended X-ray absorption fine-structure spectroscopy further revealed that SLR led to > 3 times less Fe oxide-C coprecipitates than Control conditions. In addition, the overall global warming potential (GWP) decreased under SLR due to suppressed CO_2 emissions. Our data suggest that SLR may increase lateral C export of current C stocks by dissolving C-bearing Fe oxides but decrease the overall GWP from emissions of soil trace gases. These findings have implications for understanding the fate of SOC dynamics under future SLR scenarios.

Keywords Organo-mineral associations · Lateral carbon fluxes · Synchrotron · Greenhouse gas fluxes · Dissolved organic carbon · Vertical carbon fluxes

Introduction

Tidal salt marshes are important carbon (C) reservoirs at the terrestrial-aquatic interface, but the fate of these “Blue C” stocks may be affected by sea level rise (SLR). Blue C ecosystems have soil C sequestration rates orders of magnitude greater than inland forests (Chmura et al. 2003; Mcleod et al. 2016). High plant productivity, slow decomposition, and high sedimentation rates (Arias-Ortiz et al. 2018) make tidal salt marshes an ideal C storage sink (Alongi 2020). Along with the anaerobic conditions

Responsible Editor: Christian Lønborg.

Supplementary Information The online version contains supplementary material available at <https://doi.org/10.1007/s10533-023-01024-z>.

S. Fettrow · R. Vargas · A. L. Seyfferth (✉)
Department of Plant and Soil Sciences, University
of Delaware, Newark, DE, USA
e-mail: angelias@udel.edu

that slow decomposition rates, the complex nature of marsh-derived C (Osburn et al. 2015) and the association of C with soil minerals (Sun et al. 2019); salt marshes contribute an estimated 6.5 Pg of soil C stock (Chmura et al. 2003; Bridgman et al. 2006; Duarte et al. 2013). Despite the importance of salt marsh C sequestration, these ecosystems are being lost to land use-change at an annual rate of 1–2% each year (Duarte et al. 2008), while SLR is also expected to cause widespread marsh loss. Modeling and meta-analysis have shown that SLR may completely submerge much of the existing salt marshes, decreasing blue C stocks (Valiela et al. 2018), unless enough accommodation space is available for marsh migration (Schuerch et al. 2018). Consequently, it is critical to understand how SLR will alter soil C retention and stabilization mechanisms in current salt marsh soil C stocks.

Soil minerals stabilize C through physiochemical associations, but SLR may affect this process. In particular, Fe oxides, hydroxides, and oxyhydroxides (hereafter referred to collectively as Fe oxides) are common soil minerals that protect organic C via adsorptive processes (Saidy et al. 2015). A previous study illustrated that approximately 21% of all organic C in natural systems is directly bound to reactive Fe minerals (Lalonde et al. 2012). C-bearing Fe oxides have been extensively studied in noncoastal systems (Chen and Sparks 2015; Saidy et al. 2015; Sowers et al. 2018a; Wordofa et al. 2019; Huang et al. 2020) but there has been limited study into the importance of this C retention mechanism in blue C settings. Previously, Seyfferth et al. (2020) showed that the main Fe oxide found in salt marsh high marsh soils is ferrihydrite, which is a poorly crystalline Fe oxide with a high surface area that can form strong Fe–C associations (Gu et al. 1995). These reactive Fe oxides can be reductively dissolved by Fe-reducing bacteria under sub- to anoxic conditions, releasing mineral-associated C into the porewater along with reduced Fe (Fe^{2+}) (Riedel et al. 2013; Wordofa et al. 2019). Possible changes to C-bearing Fe oxides under SLR conditions include increased reductive dissolution and decreased mineral precipitation, thereby increasing the mobility and lateral transport of current C stocks from salt marsh soils.

Changes to the stability of C-bearing Fe oxides in tidal salt marshes may alter the mobility of soil C, affecting the lateral C flux. While the vertical

C flux encompasses the flow of C into marsh vegetation and storage in the soil, the lateral C flux is characterized as the import and export of C via tidal channels (Trifunovic et al. 2020; Santos et al. 2021). Until recently, the lateral flux has been ignored, leading to potential underestimation of net C flux from coastal wetlands (Santos et al. 2021). This underestimation may be important, particularly because evidence suggests the lateral C flux may exceed the vertical C flux in these ecosystems (Wang et al. 2016; Bogard et al. 2020; Czapla et al. 2020). While the uncertainty in the lateral C flux of tidal wetlands remains high (Cavallaro et al. 2018), the effect of SLR may add an additional layer of complexity. Changes to the lateral C flux may occur if SLR increases the mobility of previously mineral-stabilized soil C. This effect of SLR on the lateral C flux and current C stocks of marsh soils remains unresolved and is needed for proper representation in earth system models (Ward et al. 2020).

SLR may also affect the emission of greenhouse gases (GHGs) via multiple pathways (Capooci et al. 2019; Luo et al. 2019). An increase in the extent of inundation may alter the exchange of GHGs from marsh soils to the atmosphere by decreasing soil redox potentials and slowing respiration rates (Hackney 1987; Chambers et al. 2013; Capooci and Vargas 2022a). While respiration rates may be slower, C may be more bioavailable under flooded conditions due to decreased mineral protection under low redox conditions, increasing GHG flux even under anoxia (Huang et al. 2020). Furthermore, SLR may decrease methane (CH_4) emissions due to enhanced sulfate reduction and microbial competition for substrate (Poffenbarger et al. 2011). However, recent work has shown methanogenesis in tidal marshes is active at depth via a methylotrophic pathway in which sulfate-reducing bacteria do not compete with methanogens for substrate (Seyfferth et al. 2020). Methane fluxes are also often controlled by the balance between rates of methanogenesis (production of CH_4) versus methanotrophy (consumption of CH_4) (Deborde et al. 2010), which may be impacted by SLR. Furthermore, tidal salt marsh soils have recently been attributed as acting as a net sink for nitrous oxide (N_2O) (Capooci and Vargas 2022b), though it is unclear how this process of nitrification in salt marshes will be affected by SLR. It is therefore important to understand how SLR will affect various GHG fluxes (i.e., carbon dioxide

(CO₂), CH₄, N₂O) and the cumulative global warming potential (GWP) from salt marsh soils.

Our main goal was to investigate how SLR impacts C-bearing Fe oxides and GHG flux in salt marsh soils. This study focuses on soils from a high marsh area near a creek channel that currently experiences flooding only once every 2 weeks due to spring tides, but is highly vulnerable to continuous inundation from SLR (Guimond et al. 2020). To isolate the impacts of SLR on C in marsh soils, we established a laboratory experiment using flow-through mesocosms subjected to two treatments: either to water-table fluctuation similar to established high marsh hydrology on a spring-neap tidal cycle (hereafter referred to as Control) or to continuous inundation (hereafter referred to as SLR). We hypothesize that (1) porewater DOC and lateral DOC export will be higher in the SLR treatment due to lower redox potential and more reductive dissolution of C-bearing Fe oxides, leading to greater DOC mobilization, and (2) increased DOC mobility will lead to greater microbial bioavailability and thus increase GHG emissions (i.e., CO₂, CH₄, N₂O) under SLR conditions. This study suggests that SLR will significantly impact the stability of existing soil C stocks in marsh soils by destabilizing Fe mineral-associated C and altering both the lateral C flux and vertical GHG fluxes.

Materials and methods

Study site and soil sampling

Soils were collected from the St. Jones National Estuarine Research Reserve, a temperate tidal salt marsh in the Mid-Atlantic region. This ecosystem has daily tidal influence from the nearby waterbodies, including the St. Jones River, which drains into the Delaware Bay (Fig. 1). The tidal creek has a salinity range of 5–18 ppt (Capooci et al. 2019). Vegetation consists primarily of *Spartina alterniflora*, with patches of *S. patens* and *S. cynosuroides*. Soils were collected in the high marsh area near a creek channel that is dominated by *S. cynosuroides*. The soils in this location are rarely continuously inundated and instead experience large spring-neap tidal oscillations. During spring tides, the soils are inundated but otherwise drain to as much as – 25 cm below the soil surface, causing wide ranges in porewater redox potentials from 0 to

700 mV (Seyfferth et al. 2020). Previous modeling efforts have suggested that this area is prone to continuous inundation under future SLR scenarios (Guimond et al. 2020).

To test how SLR will affect these soils, ten intact field moist soil cores (3 cm diameter) were taken from the 0–8 cm depth in December 2019. Cores were taken with a semi-cylindrical gouge auger which has been shown to be effective at minimizing compaction (Smeaton et al. 2020). To preserve the low-oxygen conditions at the time of collection, each core was placed into individual gas-impermeable bags with oxygen scrubbers (Mitsubishi Anaero-Pack) during transport back to the laboratory on ice. The gas-impermeable bags with the soils were stored at 4 °C for 25 days until the beginning of the experiment. While slight changes in temperature and holding times can possibly lead to changes in the microbial community, past work has shown that these changes are minimal, (Lauber et al. 2010; Rubin et al. 2013), and the holding temperature (4 °C) was not much lower than the temperature of the creek water (8 °C) at the time of collection. Moreover, all soil cores were treated the same, so any slight changes that could have occurred would have been uniform across treatments.

Soil characterization

A subsample of a randomly selected soil core from both Control and SLR was taken before (pre-treatment) and after the experiment (post-treatment) to characterize changes in the solid phase due to treatment. Each subsample (n=4) was dried, ground, and sieved to 2 mm inside an anoxic glove bag. These subsamples were further powdered and analyzed for total C (Vario EL Cube, Elementar) and total Fe with X-Ray fluorescence (Titan Handheld, Bruker). Furthermore, subsamples were used for X-ray diffraction (D8 XRD, Bruker) and Fe minerals were identified using software (Match!, Version 3.14). Fe extended X-ray fine structure (Fe EXAFS) were used to further characterize Fe mineralogy. Bulk Fe EXAFS were conducted at the National Synchrotron Light Source II on beamline 6BM. Fe K-edge spectra were obtained in transmission mode and three scans per sample were obtained and averaged in Athena (Ravel and Newville 2005). The averaged spectra were background



Fig. 1 Map of the study site location at the St Jones Reserve in Dover, Delaware. The coring location for this experiment is located close to a tidal channel. This high marsh location expe-

riences a spring-neap flooding cycle characterized by a flooding event only every 2 weeks, and soils were saturated upon collection

subtracted, normalized, and fit with a spline function ($k\text{-weight}=3$). The normalized spectra were then fit using linear combination (k -range of $2\text{--}10 \text{ \AA}^{-1}$) to known standards of the minerals that were constrained by XRD. The minerals included in the EXAFS fits were jarosite($\text{NaFe}(\text{SO}_4)_2(\text{OH})_3$), siderite(FeCO_3), magnetite(Fe_3O_4), green rust($\text{Fe(OH)}_2\text{Cl}$) and a ferrihydrite(FeOOH)-galacturonic acid coprecipitate (hereafter referred to as Fh-C coprecipitate) from previous work (ThomassasArrigo et al. 2019). The goodness of fit of the linear combination on the raw data was assessed using the reduced χ^2 and the R-value developed in Athena (Ravel and Newville 2005) and was also assessed by visually inspecting the raw data and linear combination fit data.

Flow-through soil incubation

To test our hypotheses that SLR will alter marsh soil C, ten polyethylene soil flow-through mesocosms ($7.5 \text{ cm} \times 15 \text{ cm}$) were constructed with inflow and outflow ports (Fig. S1a). The outflow port was screened with a nylon mesh to minimize soil loss. Before placing the ten soil cores into the flow-through mesocosms, 2 cm (or $\sim 300 \text{ g}$) of acid-washed coarse sand was added to the bottom of the mesocosms to avoid outflow clogging. We collected water from the nearby tidal channel at the study site to maintain the desired water levels in the mesocosms as performed in other salt marsh incubation studies (Capooci et al. 2019). The mesocosms were placed into an incubation system that was maintained at 24°C without

light nor plants to avoid confounding effects to the main hypotheses. Ten flow-through mesocosms were used to simulate SLR ($n=5$) and Control ($n=5$) treatments, acknowledging that laboratory controlled mesocosms do not fully replicate field conditions, particularly the addition of sedimentation. After quality assurance and quality control of the experimental data, we decided to only use nine mesocosms for SLR ($n=5$) and Control ($n=4$) treatments. The total duration of the experiment was 66 days.

SLR mesocosms were continuously inundated 1 cm above the soil surface, while the Control mesocosms went through a simulated spring-neap hydro-period to represent current field site hydrodynamics. The simulation of a spring-neap oscillation was done by slowly flooding and draining the mesocosms over periods of 2-weeks (Fig. S1b). Periods of flooding are hereafter referred to as “Control-Flood” while periods of draining are referred to as “Control-Ebb”. To maintain constant flow in all ten mesocosms, tidal channel water was cycled through at approximately 0.5 ml/min using a peristaltic pump (Golander BT100s, Norcross, Georgia). Previous studies have shown the importance of maintaining hydraulic connectivity when performing hydrological manipulations in mesocosms (Petrakis et al. 2017; Northrup et al. 2018; Capooci et al. 2019). For the Control mesocosms, outflow was maintained at 0.5 ml/min while inflow was altered slightly to achieve either incremental ebb or flood dynamics. Gas-permeable Tygon tubing was used for the tidal creek water inflow tubing to allow the input water to oxygenate before entering the mesocosms while Viton tubing with a low gas permeability was used for the lateral export water to limit its exposure to the atmosphere. All flow-through mesocosms were open (i.e., not capped) to allow soil-atmosphere interactions, except during gas flux measurements described in the following section.

Measurements of greenhouse gas fluxes

To test how simulated SLR impacts GHG dynamics, soil GHGs (i.e., CO₂, CH₄, and N₂O) fluxes were measured every three days starting one day after mesocosms were flooded. We used the closed chamber approach with each flow-through mesocosm as has been done with other mesocosm experiments (Petrakis et al. 2017; Teasley et al. 2017; Capooci et al. 2019). Changes in concentrations of GHGs were

measured every 5 s for 3 min per mesocosm with a Gasmet FTIR gas analyzer (DX4040, Gasmet Technologies, Finland) outfitted with gas impermeable tubing. Flux values were calculated using the following equation:

$$\text{Soil GHG Flux} = \frac{\Delta c}{\Delta t} \frac{V}{S} \frac{Pa}{RT}$$

where c is the mole fraction of CO₂, CH₄, or N₂O in $\mu\text{mol mol}^{-1}$, t is the observation time of 180 s, V is the total volume of the closed system, S is the surface area within the flow-through mesocosms, Pa is the atmospheric pressure inside the mesocosm, R is the universal gas constant, T is the surface water or surface soil temperature, and a linear fit was applied to calculate $\Delta c/\Delta t$ using an in-house code (Limmer et al. 2018). We applied a linear fit as a conservative approach and to avoid bias induced by applying an exponential fit at near-zero fluxes or negative fluxes (Barba et al. 2018).

We applied a quality assurance and quality control (QA/QC) approach to calculate GHG fluxes described in previous studies (Petrakis et al. 2017; Barba et al. 2019; Capooci et al. 2019; Capooci and Vargas 2022a, b). Briefly, when the R² value of the calculated CO₂ flux was < 0.8 we considered that the micrometeorological conditions inside the chamber were not appropriate to calculate an accurate flux. Consequently, calculations were removed for that measurement's CO₂, CH₄, and N₂O fluxes and replaced as not-a-number (i.e., NaN). When conditions inside the chamber were appropriate (R² value > 0.8 for CO₂), we kept flux calculations of all three GHGs under the assumption that appropriate micrometeorological conditions were achieved for that measurement. Out of 189 flux measurements taken, only 59 did not pass our QA/QC thresholds. These 59 measurements were not used in further analyses and demonstrate the importance of having a strict QA/QC protocol.

Global warming potentials (GWPs) for 20 and 100-year scenarios were calculated from the obtained flux values by multiplying the cumulative sum (g m⁻² day⁻¹) of each daily average CH₄ or N₂O flux by the respective 20-year and 100-year GWP scenarios (86 and 34 for CH₄, 268 and 298 for N₂O) following previous studies (Myhre et al. 2014; Petrakis et al. 2017; Capooci and Vargas 2022b) to convert CH₄ and N₂O to CO₂-equivalents of radiative forcing. Finally, we provided the sum of the CO₂,

CH₄-CO₂-equivalents and N₂O-CO₂-equivalents to obtain the GWP of the GHG fluxes during our experiment.

Porewater and export water collection

To capture porewater from the entire soil core throughout the experiment, Rhizon samplers with a nominal pore size of 0.2 µm (Rhizosphere Research Products, product 19.21.01) were inserted into each soil core at a ~ 45° angle, ensuring that the entire sampling area was in contact with the soil, and these samplers remained in place throughout the entire experiment. These methods have been used previously in a wide range of mesocosm studies (Seyfferth and Fendorf 2012; Seyfferth et al. 2016; Teasley et al. 2017; Northrup et al. 2018; Capooci et al. 2019; Linam et al. 2022). Porewater was extracted using an evacuated bottle fitted to a needle and syringe, consistent with previous methods (Seyfferth and Fendorf 2012). Porewater sampling occurred every three days, starting after an equilibrium period of 18 days. Once porewater data collection started on day 18, GHG collection was done on the same days but before porewater measurements to ensure stable soil conditions for gas efflux.

Porewater was immediately aliquoted into prepared tubes within minutes of extraction to minimize sample oxidation. We placed 0.5 ml into tubes containing ferrozine reagent for Fe²⁺ analysis by the colorimetric method (Stookey 1970) and 1.5 ml was used for redox potential measurements (Orion 9179E Triode) and pH analysis (Orion Ross Ultra pH/ATC Triode) using calibrated probes. The remaining porewater sample were split for conductivity (Orion DuraProbe Conductivity Cell) and dissolved organic carbon (DOC) analysis. Conductivity was converted to salinity in part per thousand (ppt) using the conversion factor: salinity(ppt) = (conductivity(ms/cm)^{1.0878}) × (0.4665). For DOC analysis, porewater was placed into acid washed glass vials, diluted with 5.0 ml of double deionized water, and acidified with 0.1 ml of 6 M HCl (pH < 4.0) to drive off inorganic C and to inhibit microbial activity. DOC samples were frozen until analysis. In addition to porewater, 4.0 ml of lateral export water was collected from the outflow port of the flow-through mesocosm approximately every 6 days starting after the 18-day equilibrium period. These lateral export water samples were

filtered through 0.7 µm glass fiber filters (Whatman GF/F) and prepared for DOC analysis as above. Porewater and lateral DOC water samples were run on a TOC analyzer (Vario TOC Cube, Elementar) after sparging for 1 min with CO₂-free air and calibrated against known standards.

Statistical analysis

Repeated measurements analysis of variance (ANOVA) was performed when testing for significant differences between the Control and SLR treatments ($\alpha=0.05$). In addition, Control was split into two groups of data: Control-Flood and Control-Ebb as previously described (Section “Flow-through soil incubation”). Splitting Control into two groups based on tidal stage allowed us to further investigate how water level change affected measured parameters. Structural equation models (SEMs) were also used to test for hypothesized relationships between porewater variables and lateral DOC export (Harlow 2002). This statistical method can be seen as a multiple regression approach in which interactions and nonlinearities are accounted for by a hypothesized model (Fan et al. 2016). We tested a hypothetical model based on a mechanism in which SLR will decrease soil redox potential, increase Fe reduction, thereby increasing the mobility and lateral flux of DOC (Fig. S2). Data used to parameterize this model includes both porewater (pH, redox, Fe²⁺, DOC) and lateral export DOC for both treatments and for all available dates of the experiment. All data across the 2-month experiment was used in the model. To assess the fit of our data to SEMs, we included the comparative fit index (CFI), the root mean square error of approximation (RMSEA) and the p-values. We also included these parameters for unrestricted (i.e., best fitting model) and independence models (i.e., worst fitting model). All statistical analyses were performed using JMP Pro 16 (Version 16.2).

Results

Soil characterization

The total soil C and Fe concentrations were approximately 4% pre-treatment, with a C:Fe ratio of 1.00 (Table 1). Post-treatment, the C:Fe ratio increased

Table 1 Total C and Fe for soil samples, along with linear combination fitting results of Fe EXAFS spectra from sediment used in the incubation study

Sample	C (%)	Fe (%)	C:Fe ratio	% mineral-species					Reduced χ^2	R value
				FHY-GA	SID	JAR	GR	MAG		
Control Pre	3.68	3.71	1.00	24	16	36	18	6	0.38	0.08
Control Post	3.43	3.00	1.14	37	18	31	6	8	0.44	0.09
SLR Pre	4.01	4.02	1.00	25	17	37	16	6	0.31	0.07
SLR Post	4.33	3.86	1.12	29	14	35	17	5	0.32	0.07

Reduced χ^2 , and R values indicate the goodness of fit for EXAFS spectra. “Pre” indicates the sample was taken before the experiment while “post” indicates the sample was taken after the experiment

FHY-GA ferrihydrite-galacturonic acid coprecipitate, SID siderite, JAR jarosite, GR green rust, MAG magnetite

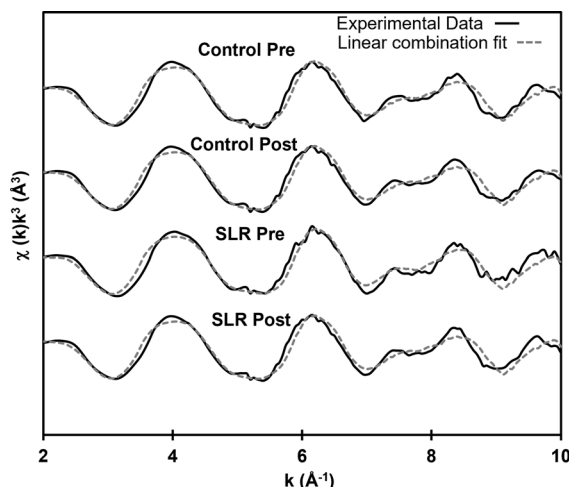


Fig. 2 Normalized iron K-edge extended X-ray absorption fine structure (EXAFS) spectra for Control and SLR pre and post treatment samples. Experimental data and linear combination model fits (k -range of $2\text{--}10 \text{ \AA}^{-1}$) are shown as solid and dashed lines, respectively

by 14% in Control and 12% under SLR. Fe minerals were identified with XRD (jarosite, ferrihydrite, green rust, siderite, magnetite) and the spectra were similar between pre- and post-treatment in both Control and SLR samples (Fig. S3). Fe EXAFS analysis showed that Control and SLR pre-treatment soils were similar (Fig. 2), demonstrating the homogeneity of the samples at the beginning of the experiment, and that jarosite made up the largest fraction of Fe minerals, followed by the Fh-C coprecipitate, green rust, siderite, and magnetite. However, post-treatment soils were affected by treatments where Fh-C increased by 54% under Control conditions

while increasing by only 16% under SLR conditions. This indicates that Fh-C coprecipitates increased post-treatment 3.4 times more under Control conditions than they did under SLR conditions. Siderite increased under Control conditions but decreased for SLR. Jarosite decreased in both treatments. Green rust decreased under Control conditions but increased under SLR conditions. Magnetite increased under Control conditions but decreased under SLR conditions. The change in Fe mineralogy between Control and SLR treatments, particularly the Fh-C coprecipitate, have important implications for the stability of soil C under SLR conditions.

Soil greenhouse gas fluxes

Fluxes of GHGs (Fig. 3) and the cumulative global warming potential (GWP) (Table 2) were affected by the experimental SLR treatment in different ways. The overall means were not statistically significant ($p > 0.05$) for soil CO_2 , CH_4 or N_2O fluxes because of the large temporal variability, but the cumulative sums of these GHG fluxes were different. Over the course of the experiment, both treatments were net sources of CO_2 while SLR had a lower cumulative soil CO_2 efflux by 29%. Both treatments were net sinks of CH_4 while SLR had a lower cumulative soil CH_4 flux by 225% under the 20-year GWP scenario and by 150% under the 100-year scenario. The Control treatment was a net sink of N_2O while the SLR treatment was a net source, which was an increase of approximately 900% under the 20-year and 100-year GWP scenarios. Even though N_2O and CH_4 have a much larger radiative forcing than CO_2 , cumulative

Fig. 3 GHG timeseries indicating the averages of the replicate mesocosms for both SLR and Control treatments for **a** CO₂, **b** CH₄, and **c** N₂O. The error bars indicate the standard deviation among the replicates. P-value and means are a result of repeated measures ANOVA between SLR and Control across the entire 66-day experiment. The blue background indicates the relative water level of the Control treatment, with the brackets showing periods where the water level was increasing (flood) or decreasing (ebb). Not all timepoints had enough replicates ($n < 3$) to calculate a standard deviation therefore not all points have error bars

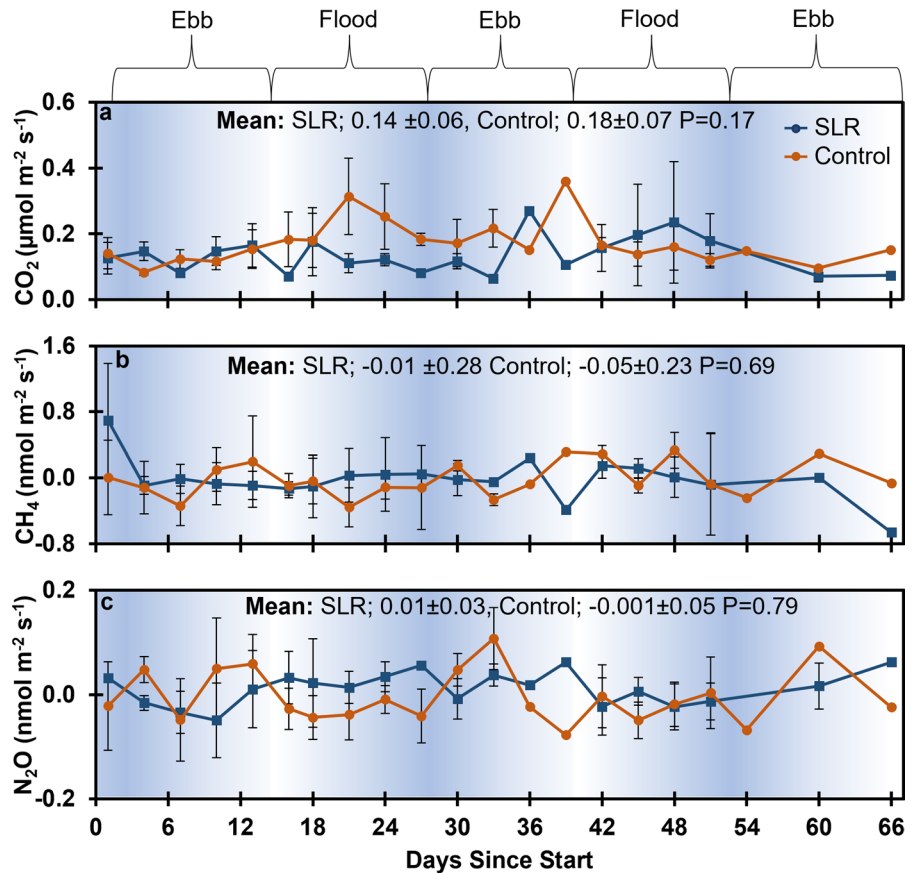


Table 2 Global warming potential (GWP) of the cumulative GHG emissions for 20 and 100-year scenarios

CO ₂ (g m ⁻²)	CH ₄ [CO ₂ eq (g m ⁻²)]		N ₂ O [CO ₂ eq (g m ⁻²)]		Total [CO ₂ eq (g m ⁻²)]	
	20-year	100-year	20-year	100-year	20-year	100-year
SLR 10.26 ± 4.15	-0.13 ± 0.58	-0.05 ± 0.23	0.73 ± 0.82	0.81 ± 0.91	10.86 ± 5.55	11.02 ± 5.29
Control 13.73 ± 1.22	-0.04 ± 0.52	-0.02 ± 0.21	-0.09 ± 0.88	-0.10 ± 0.98	13.6 ± 2.62	13.61 ± 2.41

Values indicate the GWP (\pm SD) for 20- and 100-year scenarios for each GHG

soil CO₂ efflux still comprised most of the net GWP in both treatments.

We further compared GHG flux by splitting Control treatments into Flood and Ebb stages and examined the means between SLR, Control-Ebb, and Control-Flood (Table 3). We did not find significant differences in the means of each GHG between treatments due to large temporal variability. The mean CO₂ flux was always positive for Control-Flood and Control-Ebb; fluxes of N₂O from Control-Ebb were

positive while Control-Flood was negative; and CH₄ flux was always negative for all scenarios. These results show the large temporal variability of GHG fluxes and reinforced the use of cumulative sums and GWP for this experiment.

Soil porewater and lateral export of water

SLR significantly affected porewater biogeochemical variables, as well as the lateral DOC concentration

Table 3 Summary of means for porewater, lateral DOC, and GHG flux

Parameter	SLR	Control-flood	Control-Ebb
CO_2 ($\mu\text{mol m}^{-2} \text{s}^{-1}$)	$0.14 \pm (0.10)^{\text{A}*}$	$0.19 \pm (0.10)^{\text{A}}$	$0.15 \pm (0.07)^{\text{A}}$
N_2O ($\text{nmol m}^{-2} \text{s}^{-1}$)	$0.01 \pm (0.06)^{\text{A}}$	$-0.02 \pm (0.06)^{\text{A}}$	$0.01 \pm (0.08)^{\text{A}}$
CH_4 ($\text{nmol m}^{-2} \text{s}^{-1}$)	$-0.02 \pm (0.41)^{\text{A}}$	$-0.05 \pm (0.40)^{\text{A}}$	$-0.01 \pm (0.32)^{\text{A}}$
Porewater DOC (mM)	$1.7 \pm (0.50)^{\text{A}}$	$1.3 \pm (0.40)^{\text{B}}$	$1.0 \pm (0.19)^{\text{C}}$
Lateral DOC (mM)	$0.63 \pm (0.14)^{\text{A}}$	$0.60 \pm (0.15)^{\text{AB}}$	$0.52 \pm (0.14)^{\text{B}}$
Fe^{2+} (mM)	$0.15 \pm (0.11)^{\text{A}}$	$0.09 \pm (0.09)^{\text{B}}$	$0.07 \pm (0.06)^{\text{B}}$
Redox (mV)	$214 \pm (56)^{\text{B}}$	$205 \pm (48)^{\text{B}}$	$263 \pm (53)^{\text{A}}$
pH	$7.3 \pm (0.32)^{\text{A}}$	$7.6 \pm (0.24)^{\text{B}}$	$7.6 \pm (0.31)^{\text{B}}$
Salinity (ppt)	$2.43 \pm (0.88)^{\text{A}}$	$2.67 \pm (0.76)^{\text{A}}$	$1.94 \pm (0.87)^{\text{B}}$

*Values (\pm SD) with different superscripted letters are significantly different ($p < 0.05$) based on repeated measures ANOVA analysis

(Fig. 4). Porewater Fe^{2+} mean concentration was significantly higher in SLR treatments than Control treatments by a factor of approximately two, and both decreased over time reaching a new steady state equilibrium. When the Control treatment was split into periods of ebb stage versus flood stage, (SLR, Control-Ebb, Control-Flood), SLR had the highest mean Fe^{2+} concentration, followed by Control-Flood and Control-Ebb (Table 3). Higher Fe^{2+} levels corresponded with lower redox potential. SLR treatments had significantly lower redox potentials than the Control treatments. Control-Ebb had significantly higher mean redox potential than both Control-Flood and SLR which were not significantly different from each other. While the salinity was not significantly different between Control and SLR treatments, Control-Ebb was significantly lower than SLR. In addition, salinity decreased over time and reached a new steady state equilibrium similar to the response of Fe^{2+} . Mean lateral DOC and porewater DOC levels were significantly higher under SLR conditions compared to Control. Porewater DOC concentrations are similar in concentration to DOC concentrations found at the field site (Seyfferth et al. 2020). In addition, porewater DOC mean concentrations in SLR, Control-Flood, and Control-Ebb are all significantly different from one another and decrease in concentration in that order.

Porewater, lateral export water, and GHG relationships

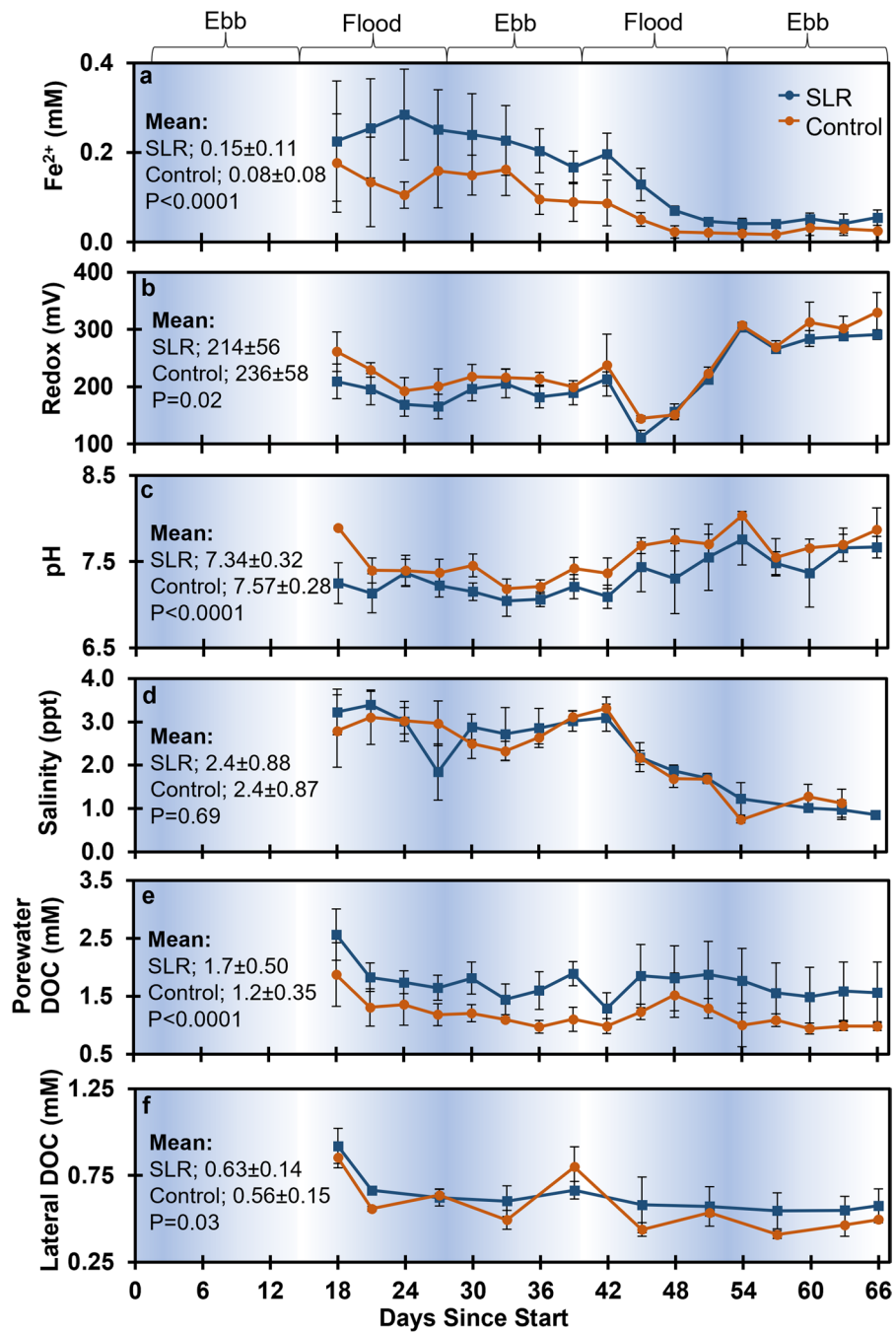
Our data show that under increased flooding conditions due to SLR, the mobility and bioavailability of DOC may increase due to increased reductive dissolution of C-bearing Fe oxides. These results are

supported by analyses exploring linear relationships and using SEMs. First, our results show positive, but weak, relationships between Fe^{2+} and lateral DOC in the SLR treatment ($R^2=0.17$, $p=0.003$) and in the Control-Flood ($R^2=0.17$, $p=0.07$), but not in Control-Ebb ($R^2=0.10$, $p=0.18$) (Fig. 5). There was a strong significant linear relationship between porewater DOC and lateral export DOC for SLR ($R^2=0.59$, $p < 0.0001$) but is weaker for the Control-Flood ($R^2=0.28$, $p=0.01$) treatment, while no such relationship exists for Control-Ebb ($R^2=0.00008$, $p=0.97$). In addition, the lateral export of DOC for SLR had a significant and positive relationship ($R^2=0.56$, $p < 0.0001$) when analyzed against Control-Flood but does not when it is analyzed against Control-Ebb ($R^2=0.11$, $p=0.16$) (Fig. 6). These results imply greater similarity between SLR and periods of Control-Flood than with periods of Control-Ebb for lateral DOC. In addition, we found statistically significant, but weak, relationships between soil CO_2 efflux and both lateral and porewater DOC, but only for SLR (Fig. 5). No significant trends were observed between the other GHGs (i.e., CH_4 , N_2O) and DOC variables. These results suggest that although linear relationships are apparent, there could be interacting or compounding effects among variables. Consequently, we tested a hypothesized model using a structural equation model (SEM) approach.

An SEM was built to test the hypothesis that SLR increases lateral DOC export by increasing reductive dissolution of C-bearing Fe oxides (parameters included pH, redox, Fe^{2+} , porewater DOC and lateral DOC; Fig. S2). We independently tested the same hypothesized model using information derived from Control or SLR treatments (i.e., two independent SEMs were tested with information from either

Fig. 4 Timeseries for Fe^{2+} (a), Redox (b), pH (c), Salinity (d), Porewater DOC (e) and Lateral DOC (f). The error bars indicate the standard deviation among the replicates.

P-value and means are a result of repeated measures ANOVA between SLR and Control treatments across the entire 66-day experiment. The blue background indicates the relative water level of the Control treatment, with the brackets showing periods where the water level was increasing (flood) or decreasing (ebb)



Control or SLR treatments). Our results show that different relationships among parameters are identified by the SEM approach (Fig. 7). The strength of the model fit was greater for SLR treatment (Table 4), suggesting that our hypothetical model is better supported using data derived from a SLR scenario. Under Control conditions, pH and porewater redox potential

significantly covary, but only pH is significantly and negatively related to Fe^{2+} , and then Fe^{2+} is positively related to porewater DOC but without a significant relationship with lateral fluxes of DOC (Fig. 7a). In contrast, under SLR conditions, pH and redox significantly covary and both are negatively related to Fe^{2+} ; consequently, Fe^{2+} and porewater DOC are positively

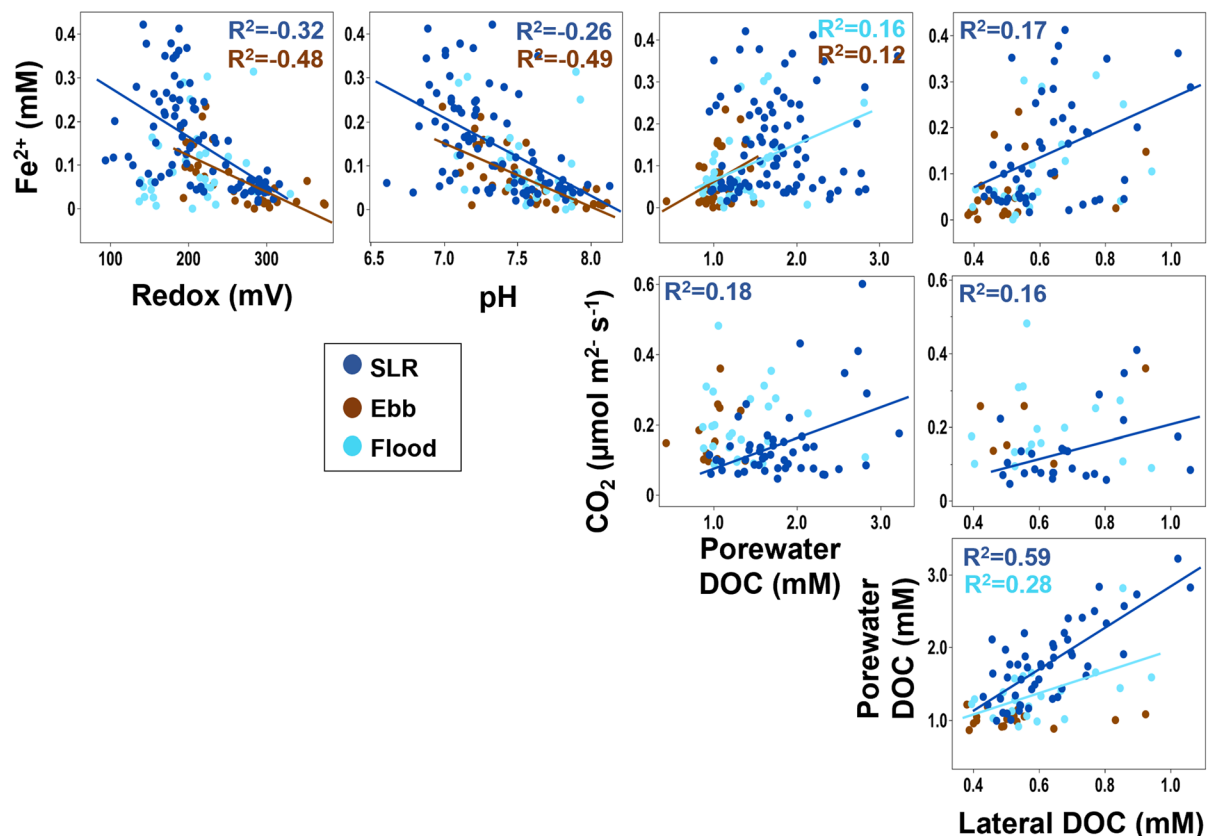


Fig. 5 Linear trend matrix between variables. The data has been grouped into SLR, Control-Flood, and Control-Ebb. R^2 values and trend lines are reported only if the relationship was significant ($p < 0.05$)

related to lateral fluxes of DOC (Fig. 7b). The SEM provides additional statistical evidence in support of our hypothesis that SLR will decrease redox, increase reductive dissolution of Fe, and increase lateral DOC export.

Discussion

Iron mineral control on DOC

Fe oxides are critical in stabilizing soil C in tidal marsh soils, as has been found for other ecosystems, but how the C-dense marsh soils will respond to SLR is still unresolved (Chen and Sparks 2015; Saidy et al. 2015; Sowers et al. 2018b; Wordofa et al. 2019; Adhikari et al. 2019; Huang et al. 2020). Here, our experimental data support the hypothesis that increased inundation under SLR conditions will lead

to soil C loss from marsh soils via reductive dissolution of C-bearing Fe oxides. Under present-day conditions (simulated here by Control treatments), soils near tidal channels drain after each tidal cycle, allowing the soils to reoxygenate during low tides. This process re-oxidizes Fe(II), forming reactive minerals such as ferrihydrite that can sequester DOC. These hydrodynamic conditions allow at least partial stabilization of porewater DOC onto newly formed Fe minerals by surface adsorption or coprecipitation, which can occur within less than 30 min of oxygen exposure (Sodano et al. 2017). While the difference in means between SLR and Control redox potential was small, SLR treatments had a significantly lower redox potential. We suspect even greater reducing conditions would have occurred with a longer experiment length. SLR treatments also had higher concentrations of porewater DOC and Fe²⁺ (Fig. 4), which suggests enhanced reductive dissolution of C-bearing

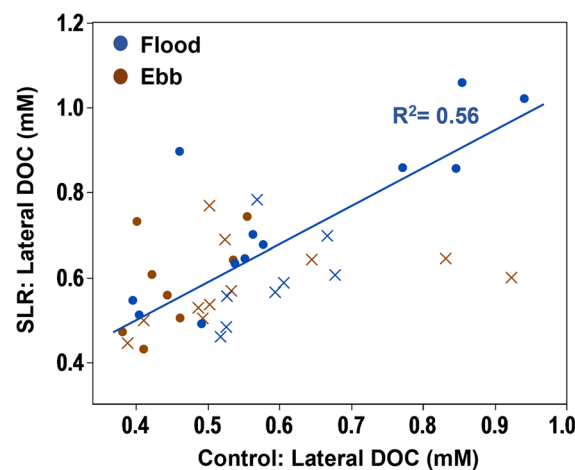


Fig. 6 Plots of export DOC for SLR verse either Control-Flood or Control-Ebb. Timepoints represented by “X” are completely flooded Control timepoints, or completely drained Control timepoints. This represents how SLR is similar to Control-Flood lateral DOC export, but not Control-Ebb. R^2 and p-value are reported only if the relationship is significant ($p < 0.05$)

Fe oxides mediated by Fe reducing bacteria (Wordofa et al. 2019). Whereas dissolution and reoxidation of Fe(II) as ferrihydrite occurs periodically as Control soils are drained and flooded, prolonged inundation caused by SLR will deplete the soils of reactive ferrihydrite as it dissolves and making surface adsorption or coprecipitation of DOC with Fe oxides less likely. This is supported by our Fe EXAFS data, as post-treatment SLR soils contained 3.4 times less Fh-C coprecipitate than post-treatment Control soils. Note that even though both treatments had decreasing porewater Fe(II) concentrations over time likely due to loss of reactive ferrihydrite minerals, this loss was more pronounced with SLR treatments. Thus, C destabilization appears to have been promoted under SLR treatments as reductive dissolution of C-bearing Fe oxides progressed because solution-phase DOC is more prone to microbial degradation (Huang et al. 2020) and/or transport from the system.

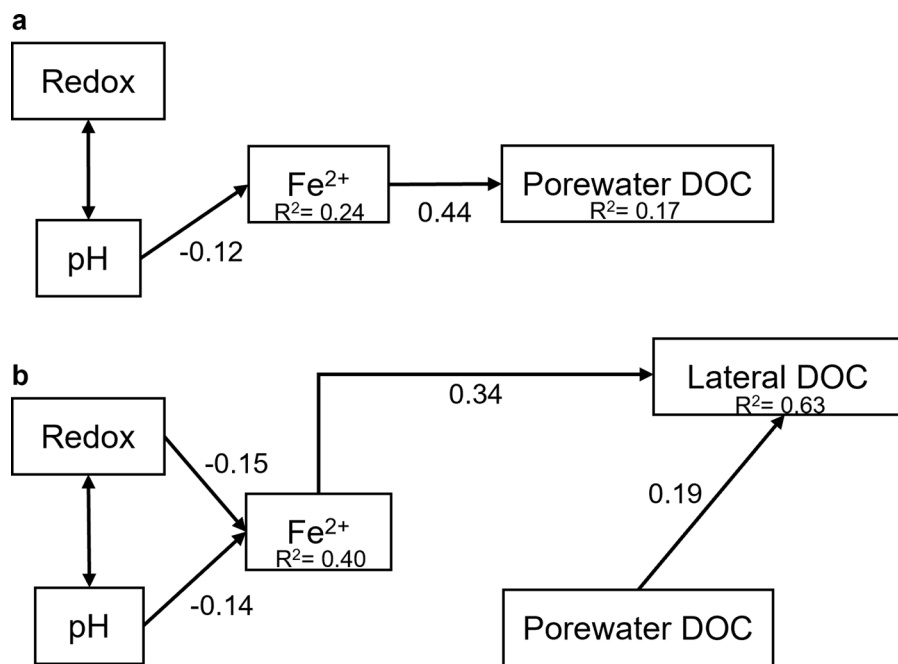


Fig. 7 Structural equation model (SEM) diagram depicting relationships between measured variables for Control (a) and SLR (b) treatments. Values on the arrows are estimates for the relationships (i.e., Change in X of 1 unit causes this estimated amount of change in Y). R^2 values are also provided for each significant ($p < 0.05$) regression. Single-sided arrows represent a hypothesized regression in the direction of the arrow, while double-sided arrows indicate covariance between two variables. We tested the same hypothetical model using SEMs parameterized with information derived either from Control or SLR treatments and here we present the final models

sent a hypothesized regression in the direction of the arrow, while double-sided arrows indicate covariance between two variables. We tested the same hypothetical model using SEMs parameterized with information derived either from Control or SLR treatments and here we present the final models

Table 4 Structural equation model (SEM) parameter output values

a. Model name	CFI	RMSEA	Prob > χ^2
Unrestricted model	1.0	0.0	
Independence model	0.0	0.29	< 0.0001
Control model	0.72	0.24	0.0004
b. Model name	CFI	RMSEA	Prob > χ^2
Unrestricted model	1.0	0.0	
Independence model	0.0	.35	< 0.0001
SLR model	0.98	0.07	0.22

CFI cumulative fit index; RMSEA root mean squared error approximation; Prob > χ^2 = Significant ($p < 0.05$) difference between experimental data and model output

SLR conditions increase DOC export

Our data support the hypothesis that SLR conditions may increase the lateral export of DOC. On average, SLR treatments across the 2-month study exported $12.5 \pm 33\%$ more lateral DOC than Control treatments. While the differences between SLR and Control were small, they were significant, even in this relatively short-term experiment. Longer-term studies coupled with field investigations that include the added complexity of plant activity and sediment additions are warranted to determine if even larger changes could be observed as SLR progresses. For example, plants will add more C, but SLR will submerge plants and possibly increase C export. In our experiment, prolonged flooding led to greater DOC mobility and removal from the soil. The univariate linear analyses and the SEMs suggest that DOC builds up in the porewater under flooded conditions, is more likely to be exported from the soil, and that lateral transport of DOC may increase with SLR under future climate scenarios.

The fate of laterally exported C is difficult to determine, but pathways may include transport to adjacent estuaries or the coastal ocean where the C is either preserved outside the ecosystem or broken down and returned to the atmosphere as CO₂ or CH₄. Tidal creeks are hotspots for CO₂ and CH₄ flux, particularly during ebb tide (Trifunovic et al. 2020) when the largest lateral transport of C from marsh soils to the tidal channel is expected (Xin et al. 2011). This suggests that a fraction of C, which is laterally transported, may be immediately returned to the atmosphere, and another fraction may be transported to coastal waters and buried in shelf sediments (Duarte

2017; Najjar et al. 2018). Understanding how SLR will affect the mechanisms and patterns of lateral C is critical because up to 80% of the net CO₂ uptake in salt marshes could be laterally exported to adjacent waters (Santos et al. 2021). There are large uncertainties about how much C is exchanged laterally, returned to the atmosphere, or buried in coastal ecosystems as part of the global C cycle (Cavallaro et al. 2018). While the uncertainty of lateral C fluxes in tidal wetlands remains high (Cavallaro et al. 2018), our data show that patterns in hydrologic oscillation (spring-neap vs continuously flooded) can significantly alter DOC mobility and the lateral DOC flux from marsh soil. Therefore, changes and differences in hydrologic oscillation could be a source of uncertainty found in current lateral C flux estimates. We propose that future lateral C estimates should consider the effects of altered hydrologic oscillation on C transport, particularly in areas most vulnerable to SLR.

Soil greenhouse fluxes altered by SLR

Our data do not support the hypothesis that soil GHG fluxes would increase under SLR conditions due to greater DOC bioavailability under flooded conditions. While we observed a positive and significant relationship between porewater DOC and soil CO₂ flux under experimental SLR conditions, this treatment overall had a lower cumulative GWP due mostly to decreased soil CO₂ efflux. Our data indicate that although prolonged flooding may increase DOC bioavailability as it becomes released from the mineral-phase, as was observed in other work (Huang et al. 2020), the decreased oxygen during soil flooding limits aerobic

microbial respiration and supports anaerobes that respire more slowly (Raich and Schlesinger 1992). Thus, the potential C losses by increased DOC during inundation were partially compensated for by decreased heterotrophic respiration and lower CO₂ diffusion as a result of flooding. In addition, increased lateral export under SLR conditions may have decreased the amount of labile DOC available for microbes, which could have decreased heterotrophic respiration. We conclude that while SLR could affect microbial and physical processes in different ways, the overall impact in our experiment is a decreased GWP due mainly to suppressed soil CO₂ efflux.

There is a discrepancy in the literature about how SLR will impact CH₄ fluxes from coastal wetlands (Capooci et al. 2019; Luo et al. 2019). Some studies suggest increased salinity will have inhibitory effects on CH₄ production (Poffenbarger et al. 2011), while increased inundation frequency may increase anaerobic conditions and thus increase methanogenesis (Mueller et al. 2020). Furthermore, automated measurements (i.e., hourly resolution) have shown the complexity of the influence of tidal flooding on the temporal patterns and pulse emissions (i.e., hot-moments) of soil trace gas fluxes in salt marshes (Capooci and Vargas 2022a, b). While our SLR treatment cumulatively emitted less soil CH₄ than Control, both treatments acted as net CH₄ sinks, were not statistically different, and their CH₄ contributed little to the overall GWP. Methane consumption by soils (i.e., net CH₄ sink) may result from both anaerobic and aerobic oxidation of CH₄ (Hoehler et al. 1994), both of which may have been occurring in our experiment. Aerobic oxidation of CH₄ requires oxygen and thus is more likely to have happened in the Control treatment. Anaerobic oxidation of CH₄ uses alternative electron acceptors in low oxygen conditions and may have occurred more so in the SLR treatments. Sulfate-mediated anaerobic oxidation of methane is thought to be the primary means of CH₄ consumption in anoxic marine settings (Knittel and Boetius 2009; Smemo and Yavitt 2011), and some evidence suggests that sulfate-mediated anaerobic oxidation of CH₄ is also active in brackish coastal wetland sediments (Segarra et al. 2013). Other pathways that may be decoupled from sulfate-mediated oxidation of CH₄ include the use of Fe oxides as the terminal electron acceptor instead of sulfate (Segarra et al. 2013; Cai

et al. 2018); both processes may have occurred in the SLR treatments here. Taken together, our data suggest that CH₄ oxidation is active in the surface soils collected for this experiment.

In this experiment we focused on current C stocks in soil, so we did not include plants to avoid confounding effects regarding inputs of organic matter and plant influences on CO₂ and CH₄ efflux. We isolated the effect of soils to test the main hypothesis of this study, but we recognize that addition of plants in the experiment would likely increase the fluxes of CO₂ and CH₄ due to higher C inputs from root exudation and leaf litter. It should also be considered that future SLR conditions would eventually lead to marsh cordgrass die-off and conversion to open water at our field site (Valiela et al. 2018; Guimond et al. 2020), which would lead to conditions more similar to our experimental mesocosms. Future experiments should consider long-term effects (e.g., year or multi-year) to test persistent effects of SLR on CH₄ and CO₂ dynamics in field-settings.

Fluxes of N₂O from salt marshes may also change under SLR conditions, and our data suggest that SLR alter soils from being an overall net sink to a net source of N₂O. While net differences between SLR and Control N₂O flux were not statistically significant, the cumulative emissions for SLR were positive, while for Control the cumulative emissions were negative. The consumption of N₂O is primarily controlled by denitrification, while the production of N₂O is controlled by nitrification and the balance between those processes controls whether the ecosystem is a sink or source of N₂O (Foster and Fulweiler 2016; Maavara et al. 2019). Other work with salt marsh soils also showed a transition from a net sink to net source due to increased nitrate and ammonium loading (Moseman-Valtierra et al. 2011). The availability of nitrate and ammonium is a major factor controlling N₂O flux and their bioavailability could increase under SLR conditions. For example, salt water intrusion increases the release of bioavailable nitrogen from mineral sorption sites (Widney et al. 2019). In addition, SLR conditions had lower soil redox potentials, possibly increasing the activity of anaerobic nitrifying microbes. While the cumulative emissions of N₂O transitioned from a sink to source under the SLR treatment tested here, N₂O contributed little to the overall GWP scenarios. Future studies that involve multi-year experiments on the effects of SLR

are warranted to fully understand the effects of SLR on multiple GHGs from tidal salt marshes.

Conclusions

SLR is expected to alter C cycling in tidal salt marshes, particularly in vulnerable low-elevation coastal areas around the world. Fe oxides may stabilize a substantial amount of existing soil C stocks through physiochemical protection, but how SLR will affect their stability is unresolved. Our simulated SLR mesocosm experiment indicates that C-bearing Fe oxide minerals in marsh soils may be destabilized with increased inundation, releasing DOC to solution where it can be acted upon by soil microbes or be exported from the system. Our data suggest that the most reactive Fe minerals were consumed first and that SLR treatments reached a new steady state over time, but always had higher porewater Fe^{2+} than Control treatments. By the end of the experiment, SLR treatments had $>3\times$ less C-bearing ferrihydrite than Control, which produced new ferrihydrite with each tidal oscillation that could sequester C and slow its release. However, despite SLR leading to more DOC release, the amount was small, and the low-oxygen conditions resulted in less energetically favorable microbial metabolisms that ultimately led to decreased GWP from SLR-treated soils.

As currently oxidized high marsh areas become further inundated from SLR, the soils may lose Fe oxides through reductive dissolution and limited periods of soil oxygenation, allowing the 6.5 Pg of soil C stock in tidal marsh soils to become more vulnerable to lateral transport and degradation. If soils become permanently reducing, the ability for redox sensitive minerals to hold onto freshly produced soil C may become increasingly diminished in the future, thereby decreasing soil C stocks, but increasing the lateral C flux. High surface area soil minerals that are prone to reduction (ferrihydrite) could be flushed from the system, drastically decreasing the C holding capacity of these efficient C sinks. It is possible that other coastal wetlands such as mangroves may also be susceptible to removal of mineral-associated C under SLR conditions. Management strategies that mitigate the effects of prolonged inundation due to SLR, and preserve natural tidal cycles, may help decrease this vulnerability of mineral-associated C in coastal wetlands.

Future studies should further examine the vulnerability of mineral-associated C and changes to GHG flux under SLR conditions, particularly with long-term studies in a variety of coastal ecosystems.

Acknowledgements We thank Chloe Kroll for sampling assistance, UD Soil Testing Laboratory for analytical assistance, Bruce Ravell for beamline assistance, Laurel Thomas Arrigo for the use of a ferrihydrite-galacturonic acid coprecipitate standard for Fe EXAFS, and the staff of the Delaware National Estuarine Research Reserve (DNERR). A.L.S. acknowledges support from the National Science Foundation Grants #1759879 and #2012484, S.F. acknowledges support from the Delaware Environmental Institute, and R.V. acknowledges support from the National Science Foundation grant #1652594 and U.S. Department of Energy (DOE) grant #DE-SC0023099 and #DE-SC0022185. Parts of this research used the BMM (6-BM) Beamline of the National Synchrotron Radiation Lightsource II, an Office of Science User Facility operated for the DOE Office of Science by Brookhaven National Laboratory under Contract No. DE-SC0012704. The authors acknowledge the land on which they conducted this study is the traditional home of the Lenni-Lenape tribal nation (Delaware nation).

Author contributions All authors contributed to the study conception and design. Material preparation, data collection, and analysis were performed by SF. The first draft of the manuscript was written by SF and ALS with edits by RV. All authors commented on previous versions of the manuscript. All authors read and approved the final manuscript.

Funding A.L.S. acknowledges support from the National Science Foundation Grants #1759879 and #2012484, S.F. acknowledges support from the Delaware Environmental Institute, and R.V. acknowledges support from the National Science Foundation grant #1652594 and U.S. Department of Energy (DOE) Grants #DE-SC0023099 and #DE-SC0022185.

Data availability The datasets used for this study are available in Figshare (10.6084/m9.figshare.21989984).

Declarations

Competing interests The authors have no relevant financial or non-financial interests to disclose.

References

- Adhikari D, Sowers T, Stuckey JW et al (2019) Formation and redox reactivity of ferrihydrite-organic carbon-calcium co-precipitates. *Geochim Cosmochim Acta* 244:86–98. <https://doi.org/10.1016/j.gca.2018.09.026>
- Alongi DM (2020) Carbon balance in salt marsh and mangrove ecosystems: a global synthesis. *J Mar Sci Eng* 8:767. <https://doi.org/10.3390/jmse8100767>

- Arias-Ortiz A, Masqué P, García-Orellana J et al (2018) Reviews and syntheses: 210Pb-derived sediment and carbon accumulation rates in vegetated coastal ecosystems—setting the record straight. *Biogeosciences* 15:6791–6818. <https://doi.org/10.5194/bg-15-6791-2018>
- Barba J, Cueva A, Bahn M et al (2018) Comparing ecosystem and soil respiration: review and key challenges of tower-based and soil measurements. *Agric for Meteorol.* <https://doi.org/10.1016/j.agrformet.2017.10.028>
- Barba J, Poyatos R, Vargas R (2019) Automated measurements of greenhouse gases fluxes from tree stems and soils: magnitudes, patterns and drivers. *Sci Rep.* <https://doi.org/10.1038/s41598-019-39663-8>
- Bogard MJ, Bergamaschi BA, Butman DE et al (2020) Hydrologic export is a major component of coastal wetland carbon budgets. *Glob Biogeochem Cycles* 34:1–14. <https://doi.org/10.1029/2019GB006430>
- Bridgman SD, Megonigal JP, Keller JK et al (2006) The carbon balance of North American wetlands. *Wetlands*. [https://doi.org/10.1672/0277-5212\(2006\)26\[889:TCBONA\]2.0.CO;2](https://doi.org/10.1672/0277-5212(2006)26[889:TCBONA]2.0.CO;2)
- Cai C, Leu AO, Xie G-J et al (2018) A methanotrophic archaeon couples anaerobic oxidation of methane to Fe(III) reduction. *ISME J* 12:1929–1939. <https://doi.org/10.1038/s41396-018-0109-x>
- Capooci M, Vargas R (2022a) Diel and seasonal patterns of soil CO₂ efflux in a temperate tidal marsh. *Sci Total Environ* 802:149715. <https://doi.org/10.1016/j.scitotenv.2021.149715>
- Capooci M, Vargas R (2022b) Trace gas fluxes from tidal salt marsh soils: implications for carbon–sulfur biogeochemistry. *Biogeosciences* 19:4655–4670. <https://doi.org/10.5194/bg-19-4655-2022>
- Capooci M, Barba J, Seyfferth AL, Vargas R (2019) Experimental influence of storm-surge salinity on soil greenhouse gas emissions from a tidal salt marsh. *Sci Total Environ* 686:1164–1172. <https://doi.org/10.1016/j.scitotenv.2019.06.032>
- Cavallaro N, Shrestha G, Birdsey R et al (2018) Second state of the carbon cycle report. Washington, DC
- Chambers LG, Osborne TZ, Reddy KR (2013) Effect of salinity-altering pulsing events on soil organic carbon loss along an intertidal wetland gradient: a laboratory experiment. *Biogeochemistry* 115:363–383. <https://doi.org/10.1007/s10533-013-9841-5>
- Chen C, Sparks DL (2015) Multi-elemental scanning transmission X-ray microscopy-near edge X-ray absorption fine structure spectroscopy assessment of organo-mineral associations in soils from reduced environments. *Environ Chem* 12:64–73. <https://doi.org/10.1071/EN14042>
- Chmura GL, Anisfeld SC, Cahoon DR, Lynch JC (2003) Global carbon sequestration in tidal, saline wetland soils. *Glob Biogeochem Cycles* 17:1111. <https://doi.org/10.1029/2002GB001917>
- Czapla KM, Anderson IC, Currin CA (2020) Net ecosystem carbon balance in a North Carolina, USA, Salt Marsh. *J Geophys Res Biogeosci* 125:1–16. <https://doi.org/10.1029/2019JG005509>
- Deborde J, Anschutz P, Guérin F et al (2010) Methane sources, sinks and fluxes in a temperate tidal Lagoon: the Arcachon lagoon (SW France). *Estuar Coast Shelf Sci* 89:256–266. <https://doi.org/10.1016/j.ecss.2010.07.013>
- Duarte CM (2017) Reviews and syntheses: hidden forests, the role of vegetated coastal habitats in the ocean carbon budget. *Biogeosciences* 14:301–310. <https://doi.org/10.5194/bg-14-301-2017>
- Duarte CM, Dennison WC, Orth RJW, Carruthers TJB (2008) The charisma of coastal ecosystems: addressing the imbalance. *Estuar Coasts* 31:233–238. <https://doi.org/10.1007/s12237-008-9038-7>
- Duarte CM, Losada IJ, Hendriks IE et al (2013) The role of coastal plant communities for climate change mitigation and adaptation. *Nat Clim Chang* 3:961–968. <https://doi.org/10.1038/nclimate1970>
- Fan Y, Chen J, Shirkey G, et al (2016) Applications of structural equation modeling (SEM) in ecological studies: an updated review. *Ecol Process* 5:1–12. <https://doi.org/10.1186/s13717-016-0063-3>
- Foster SQ, Fulweiler RW (2016) Sediment nitrous oxide fluxes are dominated by uptake in a temperate estuary. *Front Mar Sci* 3:1–13. <https://doi.org/10.3389/fmars.2016.00040>
- Gu B, Schmitt J, Chen Z et al (1995) Adsorption and desorption of different organic matter fractions on iron oxide. *Geochim Cosmochim Acta* 59:219–229. [https://doi.org/10.1016/0016-7037\(94\)00282-Q](https://doi.org/10.1016/0016-7037(94)00282-Q)
- Guimond JA, Yu X, Seyfferth AL, Michael HA (2020) Using hydrological-biogeochemical linkages to elucidate carbon dynamics in coastal marshes subject to relative sea level rise. *Water Resour Res* 56:1–16. <https://doi.org/10.1029/2019WR026302>
- Hackney CT (1987) Factors affecting accumulation or loss of macroorganic matter in salt marsh sediments. *Ecology* 68:1109–1113. <https://doi.org/10.2307/1938385>
- Harlow L (2002) Using multivariate statistics. *Struct Eqn Model Multi J* 9:621–636. https://doi.org/10.1207/S15328007SEM0904_9
- Hoehler TM, Alperin MJ, Albert DB, Martens CS (1994) Field and laboratory studies of methane oxidation in an anoxic marine sediment: evidence for a methanogen-sulfate reducer consortium. *Glob Biogeochem Cycles* 8:451–463. <https://doi.org/10.1029/94GB01800>
- Huang W, Ye C, Hockaday WC, Hall SJ (2020) Trade-offs in soil carbon protection mechanisms under aerobic and anaerobic conditions. *Glob Chang Biol* 26:3726–3737. <https://doi.org/10.1111/gcb.15100>
- Knittel K, Boetius A (2009) Anaerobic oxidation of methane: progress with an unknown process. *Annu Rev Microbiol* 63:311–334. <https://doi.org/10.1146/annurev.micro.61.080706.093130>
- Lalonde K, Mucci A, Ouellet A, Gélinas Y (2012) Preservation of organic matter in sediments promoted by iron. *Nature* 483:198–200. <https://doi.org/10.1038/nature10855>
- Lauber CL, Zhou N, Gordon JI et al (2010) Effect of storage conditions on the assessment of bacterial community structure in soil and human-associated samples. *FEMS Microbiol Lett* 307:80–86. <https://doi.org/10.1111/j.1574-6968.2010.01965.x>
- Limmer MA, Mann J, Amaral DC et al (2018) Silicon-rich amendments in rice paddies: effects on arsenic uptake and biogeochemistry. *Sci Total Environ* 624:1360–1368. <https://doi.org/10.1016/j.scitotenv.2017.12.207>

- Linam F, Limmer MA, Tappero R, Seyfferth AL (2022) Rice husk and charred husk amendments increase porewater and plant Si but water management determines grain As and Cd concentration. *Plant Soil.* <https://doi.org/10.1007/s11104-022-05350-3>
- Luo M, Huang J-F, Zhu W-F, Tong C (2019) Impacts of increasing salinity and inundation on rates and pathways of organic carbon mineralization in tidal wetlands: a review. *Hydrobiologia* 827:31–49. <https://doi.org/10.1007/s10750-017-3416-8>
- Maavara T, Lauerwald R, Laruelle GG et al (2019) Nitrous oxide emissions from inland waters: are IPCC estimates too high? *Glob Chang Biol* 25:473–488. <https://doi.org/10.1111/gcb.14504>
- Mcleod E, Chmura GL, Bouillon S et al (2016) A blueprint for blue carbon: toward an improved understanding of the role of vegetated coastal habitats in sequestering CO₂. *Front Ecol Environ* 9:552–560
- Moseman-Valtierra S, Gonzalez R, Kroeger KD et al (2011) Short-term nitrogen additions can shift a coastal wetland from a sink to a source of N₂O. *Atmos Environ* 45:4390–4397. <https://doi.org/10.1016/j.atmosenv.2011.05.046>
- Mueller P, Mozdzer TJ, Langley JA et al (2020) Plant species determine tidal wetland methane response to sea level rise. *Nat Commun* 11:5154. <https://doi.org/10.1038/s41467-020-18763-4>
- Myhre G, Shindell D, Huang J et al (2014) Anthropogenic and natural radiative forcing. *Climate change 2013—the physical science basis*. Cambridge University Press, Cambridge, pp 659–740
- Najjar RG, Herrmann M, Alexander R et al (2018) Carbon budget of tidal wetlands, estuaries, and shelf waters of Eastern North America. *Glob Biogeochem Cycles* 32:389–416. <https://doi.org/10.1002/2017GB005790>
- Northrup K, Capooci M, Seyfferth AL (2018) Effects of extreme events on arsenic cycling in salt marshes. *J Geophys Res Biogeosci* 123:1086–1100. <https://doi.org/10.1002/2017JG004259>
- Osburn CL, Mikan MP, Etheridge JR et al (2015) Seasonal variation in the quality of dissolved and particulate organic matter exchanged between a salt marsh and its adjacent estuary. *J Geophys Res G Biogeosci* 120:1430–1449. <https://doi.org/10.1002/2014JG002897>
- Petrakis S, Seyfferth A, Kan J et al (2017) Influence of experimental extreme water pulses on greenhouse gas emissions from soils. *Biogeochemistry* 133:147–164. <https://doi.org/10.1007/s10533-017-0320-2>
- Poffenbarger HJ, Needelman BA, Megonigal JP (2011) Salinity influence on methane emissions from tidal marshes. *Wetlands* 31:831–842. <https://doi.org/10.1007/s13157-011-0197-0>
- Raich JW, Schlesinger WH (1992) The global carbon dioxide flux in soil respiration and its relationship to vegetation and climate. *Chem Phys Meteorol* 44:81–99. <https://doi.org/10.3402/tellusb.v44i2.15428>
- Ravel B, Newville M (2005) ATHENA, ARTEMIS, HEPHAESTUS : data analysis for X-ray absorption spectroscopy using IFEFFIT. *J Synchrotron Radiat* 12:537–541. <https://doi.org/10.1107/S0909049505012719>
- Riedel T, Zak D, Biester H, Dittmar T (2013) Iron traps terrestrially derived dissolved organic matter at redox interfaces. *Proc Natl Acad Sci USA* 110:10101–10105. <https://doi.org/10.1073/pnas.1221487110>
- Rubin BER, Gibbons SM, Kennedy S et al (2013) Investigating the impact of storage conditions on microbial community composition in soil samples. *PLoS ONE*. <https://doi.org/10.1371/journal.pone.0070460>
- Saidy AR, Smernik RJ, Baldock JA et al (2015) Microbial degradation of organic carbon sorbed to phyllosilicate clays with and without hydrous iron oxide coating. *Eur J Soil Sci* 66:83–94. <https://doi.org/10.1111/ejss.12180>
- Santos IR, Burdige DJ, Jennerjahn TC et al (2021) The renaissance of Odum's outwelling hypothesis in "Blue Carbon" science. *Estuar Coast Shelf Sci* 255:107361. <https://doi.org/10.1016/j.ecss.2021.107361>
- Schuerch M, Spencer T, Temmerman S et al (2018) Future response of global coastal wetlands to sea-level rise. *Nature* 561:231–234. <https://doi.org/10.1038/s41586-018-0476-5>
- Segarra KEA, Comerford C, Slaughter J, Joye SB (2013) Impact of electron acceptor availability on the anaerobic oxidation of methane in coastal freshwater and brackish wetland sediments. *Geochim Cosmochim Acta* 115:15–30. <https://doi.org/10.1016/j.gca.2013.03.029>
- Seyfferth AL, Fendorf S (2012) Silicate mineral impacts on the uptake and storage of arsenic and plant nutrients in rice (*Oryza sativa* L.). *Environ Sci Technol* 46:13176–13183. <https://doi.org/10.1021/es3025337>
- Seyfferth AL, Morris AH, Gill R et al (2016) Soil incorporation of silica-rich rice husk decreases inorganic arsenic in rice grain. *J Agric Food Chem* 64:3760–3766. <https://doi.org/10.1021/acs.jafc.6b01201>
- Seyfferth AL, Bothfeld F, Vargas R et al (2020) Spatial and temporal heterogeneity of geochemical controls on carbon cycling in a tidal salt marsh. *Geochim Cosmochim Acta* 282:1–18. <https://doi.org/10.1016/j.gca.2020.05.013>
- Smeaton C, Barlow NLM, Austin WEN (2020) Coring and compaction: best practice in blue carbon stock and burial estimations. *Geoderma* 364:114180. <https://doi.org/10.1016/j.geoderma.2020.114180>
- Smemo KA, Yavitt JB (2011) Anaerobic oxidation of methane: an underappreciated aspect of methane cycling in peatland ecosystems? *Biogeosciences* 8:779–793. <https://doi.org/10.5194/bg-8-779-2011>
- Sodano M, Lerda C, Nisticò R et al (2017) Dissolved organic carbon retention by coprecipitation during the oxidation of ferrous iron. *Geoderma* 307:19–29. <https://doi.org/10.1016/j.geoderma.2017.07.022>
- Sowers TD, Adhikari D, Wang J et al (2018a) Spatial associations and chemical composition of organic carbon sequestered in Fe, Ca, and organic carbon ternary systems. *Environ Sci Technol* 52:6936–6944. <https://doi.org/10.1021/acs.est.8b01158>
- Sowers TD, Stuckey JW, Sparks DL (2018b) The synergistic effect of calcium on organic carbon sequestration to ferrihydrite. *Geochem Trans* 19:22–26. <https://doi.org/10.1186/s12932-018-0049-4>
- Stookey LL (1970) Ferrozine—a new spectrophotometric reagent for iron. *Anal Chem* 42:779–781. <https://doi.org/10.1021/ac60289a016>
- Sun H, Jiang J, Cui L et al (2019) Soil organic carbon stabilization mechanisms in a subtropical mangrove and salt marsh

- ecosystems. *Sci Total Environ* 673:502–510. <https://doi.org/10.1016/j.scitotenv.2019.04.122>
- Teasley WA, Limmer MA, Seyfferth AL (2017) How rice (*Oryza sativa* L.) responds to elevated as under different Si-rich soil amendments. *Environ Sci Technol* 51:10335–10343. <https://doi.org/10.1021/acs.est.7b01740>
- ThomasArrigo LK, Kaegi R, Kretzschmar R (2019) Ferrihydrite growth and transformation in the presence of ferrous iron and model organic ligands. *Environ Sci Technol* 53:13636–13647. <https://doi.org/10.1021/acs.est.9b03952>
- Trifunovic B, Vázquez-Lule A, Capooci M et al (2020) Carbon dioxide and methane emissions from a temperate salt marsh tidal creek. *J Geophys Res Biogeosci*. <https://doi.org/10.1029/2019JG005558>
- Valiela I, Lloret J, Bowyer T et al (2018) Transient coastal landscapes: rising sea level threatens salt marshes. *Sci Total Environ* 640–641:1148–1156. <https://doi.org/10.1016/j.scitotenv.2018.05.235>
- Wang ZA, Kroeger KD, Ganju NK et al (2016) Intertidal salt marshes as an important source of inorganic carbon to the coastal ocean. *Limnol Oceanogr* 61:1916–1931. <https://doi.org/10.1002/limo.10347>
- Ward ND, Megonigal JP, Bond-Lamberty B et al (2020) Representing the function and sensitivity of coastal interfaces in earth system models. *Nat Commun* 11:2458. <https://doi.org/10.1038/s41467-020-16236-2>
- Widney SE, Smith D, Herbert ER et al (2019) Science of the total environment chronic but not acute saltwater intrusion leads to large release of inorganic N in a tidal freshwater marsh. *Sci Total Environ* 695:133779. <https://doi.org/10.1016/j.scitotenv.2019.133779>
- Wordofa DN, Adhikari D, Dunham-Cheatham SM et al (2019) Biogeochemical fate of ferrihydrite-model organic compound complexes during anaerobic microbial reduction. *Sci Total Environ* 668:216–223. <https://doi.org/10.1016/j.scitotenv.2019.02.441>
- Xin P, Yuan L-R, Li L, Barry DA (2011) Tidally driven multiscale pore water flow in a creek-marsh system. *Water Resour Res*. <https://doi.org/10.1029/2010WR010110>

Publisher's Note Springer Nature remains neutral with regard to jurisdictional claims in published maps and institutional affiliations.

Springer Nature or its licensor (e.g. a society or other partner) holds exclusive rights to this article under a publishing agreement with the author(s) or other rightsholder(s); author self-archiving of the accepted manuscript version of this article is solely governed by the terms of such publishing agreement and applicable law.